INNSPUB

International Journal of Biosciences | IJB |
ISSN: 2220-6655 (Print); 2222-5234 (Online)
Website: https://www.innspub.net
Email contact: info@innspub.net
Vol. 27, Issue: 3, p. 62-75, 2025

RESEARCH PAPER OPEN ACCESS

Circulating tumor cell detection using magnetic nanosensor targeting epithelial–mesenchymal transition-specific markers

Shubham Singh, Charan Singh Pawar, Nagarajan Rajendra Prasad*

Department of Biochemistry and Biotechnology, Faculty of Science, Annamalai University, Chidambaram, India

Key words: Circulating tumor cell, Epithelial-mesenchymal transition, Magnetic nanosensor, Immunofluorescence, Metastasis

DOI: https://dx.doi.org/10.12692/ijb/27.3.62-75 Published: September 09, 2025

ABSTRACT

Circulating tumor cells (CTCs) are among the major causes of cancer metastasis, and their detection is critical in the context of early diagnosis and metastatic cancer marker. Despite various advances, well established approaches for CTCs are limited. This study aimed to develop a magnetic nanosensor-based approach for detecting CTCs across multiple cancers. Herein, iron oxide magnetic nanoparticles (MNP) were fabricated and coated with silica, characterized, and functionalized with antibody for epithelial cell adhesion molecule, an epithelial–mesenchymal transition marker. Additionally, the detection efficacy of the developed nanosensor was evaluated for HT-29 and MCF-7 cancer cell lines *in vitro*. Both base-MNPs (B-MNPs) and silica-coated MNPs (C-MNPs) showed notable characteristic peaks in ultraviolet-visible and Fourier-transform infrared spectra. Field-emission scanning electron microscopy showed the structural differences, with B-MNPs exhibiting a relatively uniform spherical distribution, whereas C-MNPs showed a markedly rough morphology. The results of zeta potential (−24 and −31 mV) and particle size analyses (78 and 112 nm) for B-MNPs and C-MNPs, respectively, indicated their physicochemical stability. Additionally, confocal laser scanning microscopy showed the successful antibody functionalization on the nanoparticle surface, and immunofluorescence images showed effective detection of both HT-29 and MCF-7 cells *in vitro*, with notable differences. Altogether, the findings of this study demonstrate that the proposed nanosensor could achieve effective detection of tumor cells regarding multi-cancer detection, providing a research basis for further development of an established protocol for circulating tumor cell detection.

***Corresponding author:** Nagarajan Rajendra Prasad ✉ drprasadnr@gmail.com

INTRODUCTION

Cancer is a complex disease and one of the major global health concerns, with more than 19 million cases and 9 million mortalities reported by June 2025 (Ferlay *et al.*, 2024). In addition, factors such as malignancy exacerbate the disease condition, further increasing cancer-related mortality. Metastasis refers to the process in which cancer cells from the primary tumor migrate to different locations in the body to establish the secondary tumor (Gerstberger *et al.*, 2023). The epithelial–mesenchymal transition (EMT) is a critical event involved in metastasis; it is a dynamic biological process wherein epithelial cells lose their polarity and intercellular adhesion properties; subsequently, they acquire characteristic properties of the mesenchymal cells and exhibiting enhanced motility and invasiveness (Steinestel *et al.*, 2014; J. Yang *et al.*, 2020). Typically, EMT leads to the detachment of cancer cells from the primary tumor, allowing circulating tumor cell (CTC) generating and their invasion in surrounding tissues, ultimately introducing them to the circulation system for colonization at secondary sites (Lamouille *et al.*, 2014). Notably, this transition is regulated by various key transcription factors, including Snail, Slug, and Twist (Debnath *et al.*, 2022; Garg, 2013), and different signaling pathways, such as transforming growth factor-β, Wingless/Int1, and neurogenic locus notch homolog protein pathways (Garg, 2013; Gonzalez and Medici, 2014). Overall, EMT is intricately linked to cancer metastasis and plays a pivotal role in tumor progression and therapeutic resistance.

CTCs represent the fraction of cancer cells that are detached from the primary tumor and enter the bloodstream (circulatory system), thereby serving as critical metastasis-associated mediators. Reportedly, these cells come in existence when cells from the primary tumor undergo EMT, thereby acquiring migratory and invasive characteristics, which enable their escape from the tumor microenvironment (Pantel and Speicher, 2016; Williams, 2013).

However, following their entry in the circulation system, CTCs are exposed to carious challenges, including shear stress, immune surveillance, and detachment-induced cell death (van der Toom *et al.*, 2016; Yang *et al.*, 2024). To address such challenges, CTCs have been shown to survive through mechanisms such as clustering, coating with platelets, and the expression of stem-cell-like markers (Yang *et al.*, 2024; Zhou *et al.*, 2024), and owing to these mechanisms, surviving CTCs are migrate to distant organ sites, and upon reaching the next target site, they undergo mesenchymal–epithelial transition, thereby initiating the formation of secondary tumors (Yao *et al.*, 2011). These findings underscore the importance of CTCs, warranting extensive studies on the detection and analysis of CTCs to develop advanced approaches, such as minimally invasive liquid biopsy, for monitoring tumor progression, assessing prognosis, and guiding the therapy development (Chauhan *et al.*, 2021; Lianidou and Pantel, 2019).

Regarding CTC detection, surface markers play a crucial role in the characterization of CTCs, offering various potential targets for detection. Among them, epithelial cell adhesion molecule (EpCAM), which is a transmembrane glycoprotein, is one of the most studied CTC surface markers, and its expression is typically found on the surface of epithelial-derived tumor cells (Baeuerle and Gires, 2007; Spizzo *et al.*, 2011). Various studies have shown EpCAM is involved in cell–cell adhesion process and is overexpressed in many cancer types (Cimino *et al.*, 2010; Imrich *et al.*, 2012; Wenqi *et al.*, 2009; Zhou and Zhu, 2018).

Furthermore, it is a prominent target for the only Food and Drug Administration-approved technology for CTC enrichment in diagnostic platforms, namely the CellSearch® system (Menarini Silicon Biosystems, Inc., Huntingdon Valley, PA, USA) (Riethdorf *et al.*, 2018).

The system can target EpCAM, a major research subject implicated in many studies on CTCs, and isolates epithelial-like CTCs from blood samples for further molecular analysis.

Among various approaches being developed for CTC detection, nanoparticle-based CTC detection methods contribute to a rapidly advancing field that utilizes the unique physicochemical properties of nanoparticles to enhance the detection sensitivity, specificity, and multifunctionality in cancer diagnostics (Liu *et al.*, 2022; Myung *et al.*, 2016). To date, various nanoparticle types, including magnetic, gold, silica, and polymeric nanoparticles, have been fabricated and functionalized with different targeting ligands such as antibodies (for example, anti-EpCAM), peptides, or aptamers to selectively bind to markers on the surface of CTCs (Chang *et al.*, 2018; Cho *et al.*, 2012; Huang *et al.*, 2017; Jia *et al.*, 2021; Medley *et al.*, 2011; Opoku-Damoah *et al.*, 2018). Furthermore, various studies have developed and employed magnetic nanoparticles (MNPs) for immunomagnetic separation of CTCs and to enable their efficient enrichment and isolation under a magnetic field (Chang *et al.*, 2018; Ding *et al.*, 2016; Jia *et al.*, 2021; Kwak *et al.*, 2017; Marciello *et al.*, 2016; Zhu *et al.*, 2016). However, despite considerable advances, challenges remain in establishing standardized protocols, improving biocompatibility, and ensuring consistent performance in clinical settings. Nevertheless, nanoparticle-based approaches present substantial potential to overcome the limitations of the conventional antibody-based detection methods, research for more sensitive, rapid, and comprehensive CTC detection protocol generation for early cancer diagnosis and good prognosis. Consequently, combining EpCAM with fabricated MNPs is considered a notable strategy for comprehensive CTC detection and characterization in metastatic cancer.

Hence, the present study aimed to develop a magnetic nanosensor for enhanced CTC detection by targeting EpCAM, the EMT-specific marker. Herein, iron oxide-based MNPs were fabricated as base-MNPs (B-MNPs), which were then subjected to silica coating to generate silica-coated MNPs (C-MNPs). The MNPs were characterized for their fabrication and stability. Finally, C-MNPs were coated with EpCAM primary antibody to prepare the antibody-functionalized C-MNPs (referred to as nanosensors). Additionally, the efficacy of fabricated nanosensors was assessed *in vitro* in breast and colon cancer cell lines. The findings of this study may provide a basis for the further development of magnetic nanosensor-based protocol for cancer monitoring and metastasis risk assessment.

MATERIALS AND METHODS

Materials

Tetraethyl orthosilicate (TEOS), N-hydroxysuccinimide (NHS), and 1-ethyl-3-(3-dimethylaminopropyl)carbodiimide (EDC) were obtained from Sigma Aldrich, India. (3-Aminopropyl) triethoxysilane (APTES) was obtained from Sisco Research Laboratories Pvt. Ltd., New Mumbai, India. EpCAM primary antibody was purchased from Cell Signaling Technology. Fluorescein isothiocyanate (FITC)-labeled secondary antibody was obtained from Thermo Fisher Scientific. Phosphate-buffered saline (PBS), penicillin–streptomycin, fetal bovine serum (FBS), Dulbecco's modified Eagle medium (DMEM), 4′,6-diamidino-2-phenylindole (DAPI), trypsin, and methanol were purchased from Himedia Chemicals, Mumbai, India. A ferrite magnet was procured from the local market in Chidambaram, Tamil Nadu, India. All other reagent used were of analytical grade.

MNP preparation

B-MNP preparation

In this study, B-MNPs were prepared using the co-precipitation method (Marciello *et al.*, 2016), with some modifications. Briefly, 2 mg of $FeCl_3 \cdot 6H_2O$ and 1 mg of $FeSO_4 \cdot 7H_2O$ were added to 5 mL of distilled water and vortexed to achieve an aqueous solution with a Fe^{3+}:Fe^{2+} molar ratio of 2:1. Next, the solution was added with double volume (10 mL) of NH_4OH (25%) and mixed thoroughly. Following this, the mixture was incubated in a water bath at 80°C for 30 min to allow precipitation. The precipitate was removed using a magnet. The separated fraction was washed thrice with double-distilled water and then sonicated in three sets of 10 min each to reduce the particle size. The

sonicated particles were then placed in 5 mL of methanol and stored at 4°C until further use.

C-MNP preparation

To prepare C-MNPs, B-MNPs were subjected to silica coating. Herein, B-MNPs were removed from methanol and mixed with 80% ethanol (10 mL). They were sequentially added with TEOS and APTES, ensuring their final concentration to be 1% of the mixture. Next, the mixture was incubated for 3 h while mixing to allow silica coating and surface functionalization. After incubation, the C-MNPs were separated from the mixture and washed thoroughly with ethanol to remove unreacted reagents using a magnet. The separated fraction was washed thrice with double-distilled water, placed in 5 mL of methanol, and stored at 4°C until further use.

MNP characterization

Before functionalizing with antibody, both B-MNP and C-MNP were subjected to characterization to evaluate their successful fabrication, physicochemical properties, and stability. Both NMPs were characterized through ultraviolet-visible (UV-Vis) spectroscopy, Fourier-transform infrared (FTIR) spectroscopy, field-emission scanning electron microscopy (FESEM), energy dispersive X-ray analysis (EDAX), zeta potential analysis, and particle size analyses.

UV-Vis spectroscopy

Herein, UV-Vis spectroscopy was performed to determine the presence of fabricated MNPs using a spectrophotometer (UV-1800 UV-VIS Spectrophotometer, Shimadzu Corporation, Japan). The absorption spectra (200–1200 nm) were analyzed using the Origin 8.5 Pro software (OriginLab).

FTIR spectroscopy

FTIR spectroscopy analysis was performed using Thermo Nicolet iS5 (Thermo Fisher Scientific) to identify the chemical bonds and functional groups present on the fabricated MNPs to confirm the successful attachment of coating materials. The infrared spectra (4000–400 cm^{-1}) were analyzed using the Origin 8.5 Pro software (OriginLab).

FESEM and EDAX

FESEM was performed using the Zeiss–Sigma 300 (Carl Zeiss AG) to observe the morphology and surface structure of the fabricated B-MNPs and C-MNPs. Additionally, EDAX was performed to obtain the elemental composition data of both MNPs. The FESEM images were analyzed using the ImageJ software (ImageJ).

Zeta potential analysis

In this study, zeta potential analyses of both MNPs were performed using the Zetasizer Nano ZS90 system (Malvern Instruments, Malvern, UK) to measure the charge on their surface and evaluate their colloidal stability and aggregation potential.

Particle size analysis

Particle sizes of both B-MNP and C-MNP were analyzed using the Zetasizer Nano ZS90 system (Malvern Instruments, Malvern, UK) to determine the hydrodynamic diameter, size distribution, and uniformity of both MNPs.

Antibody functionalization of C-MNPs

Following characterization, the surface of C-MNPs were coated with EpCAM primary antibodies. Briefly, C-MNPs were extracted from methanol and added with PBS. Next, 0.5 g of NHS and 1 g of EDC were mixed at a ratio of 1:2 and added to the MNP solution, followed by 1 h of incubation, while mixing, to activate the surface for antibody conjugation.

Subsequently, 1 µL of EpCAM primary antibody was added to the solution, and the mixture was incubated for further 5 h, while mixing, to allow for antibody coating on the C-MNP surface. The generated magnetic nanosensors were separated from the mixture using the magnet and were resuspended in PBS.

Confocal laser scanning microscopy (CLSM)

Herein, CLSM was employed to visualize the fluorescence emitted by antibodies coated on the

surface of C-MNPs using NIKON- A1 MP Laser Scanning Confocal Microscope (Nikon Corporation) to confirm the successful antibody conjugation and nanosensor generation. The nanosensor with EpCAM antibody was placed on a slide, followed by the incubation with FITC-labeled secondary antibody for 1 h at 28°C. After placing the coverslip, the slide was viewed under the microscope. The obtained CLSM images were analyzed using the ImageJ software (ImageJ).

Cell culture

In this study, two cancer cell lines namely MCF-7 (breast cancer) and HT-29 (colon cancer) were used to assess the detection efficacy of the fabricated nanosensor. Both cell lines were maintained under standard conditions of 37°C in a humidified atmosphere containing 5% CO_2. The cells were cultured in DMEM supplemented with 10% FBS and 1% penicillin–streptomycin. Subculturing was performed after cells reached 70–80% confluence to ensure optimal growth and viability.

Antibody-based immunofluorescence assay

Antibody-based immunofluorescence assay was performed *in vitro* to assess if the antibody bound to cancer cells. Briefly, MCF-7 cells (10^8 cells/mL) were suspended in DMEM and plated onto a six-well plate. The plate was incubated overnight under abovementioned culture conditions (section 2.6) to allow cells to adhere. After cells were adhered, the wells were washed thrice with PBS to remove unbound cells and debris. Next, the cells were incubated overnight at 4°C with EpCAM primary antibody. After another set of three PBS washes, FITC-labeled secondary antibody was added to the wells, followed by a 1-h incubation at 28°C. The wells were again washed three times with PBS, and DAPI was added to stain nuclei and wells were incubated for 30 min in the dark at 28°C. Finally, fluorescence was observed under a fluorescence microscope (Life Technologies, USA). The images were analyzed using the Origin 8.5 Pro software (OriginLab).

Nanosensor-based immunofluorescence assay

For *in vitro* nanosensor-based immunofluorescence assay, MCF-7 and HT-29 cancer cells were employed. Briefly, the cells were (10^8 cells/mL) were suspended in PBS and subjected to 10-fold serial dilutions to prepare cell suspensions with 10^8 to 10^1 cells/mL in PBS. The diluted cell suspensions were sequentially plated onto 12-well plates and DMEM was added.

After overnight incubation to allow cells to adhere under abovementioned culture conditions (section 2.6), wells were washed thrice with PBS to remove unbound cells and debris. The adheres cells were then incubated overnight with the nanosensor, namely EpCAM antibody-functionalized C-MNP, at 4°C. Following three PBS washes, FITC-labeled secondary antibody was added to the wells, and the cells were incubated for 1 h at 28°C. These wells were again washed three times with PBS, and DAPI was added to stain nuclei, and the cells were incubated for another 30 min in the dark at 28°C. Finally, fluorescence was observed under a fluorescence microscope (Life Technologies, USA), and the fluorescence intensity was measured at 520 and 358 nm for FITC–EpCAM and DAPI using a Spectramax Microplate Multimode Reader (Molecular Devices, USA). The images were analyzed using the Origin 8.5 Pro software (OriginLab).

RESULTS

MNP preparation

Herein, following the precipitation in the water bath at 80°C, a black-colored precipitate was obtained. After sonication, when subjected to the magnetic field of the ferrite magnet, it could be seen that the black fraction moved and accumulated toward the magnet, indicating the successful fabrication of MNPs (Fig. 1). Following silica coating, C-MNP was obtained which showed attraction to the ferrite magnet, indicating that retained the magnetic properties of B-MNP were retained.

MNP characterization

UV-Vis spectroscopy

The UV-Vis spectra of both B-MNPs and C-MNPs showed similar peaks (Fig. 2), confirming their

successful formation. Notably, the peaks at 390 and 384 nm in B-MNP and C-MNP spectra, respectively, were attributed to ligand-to-metal charge transfer transitions from O^{2-} to Fe^{3+} in MNPs. Notably, in the spectra of C-MNP, the peak slightly shifted (384 nm; hypsochromic shift), which may be attributed to the silica coating. Additionally, small peaks at 262 and 272 nm were observed in B-MNP and C-MNP spectra, respectively. These secondary peaks may be because of minor interactions among the particles, with a higher peak for C-MNP (at 272 nm) attributable to the interference from the silica coating. Overall, these results showed that both B-MNPs and C-MNPs were successfully fabricated, along with the presence of silica coating in C-MNPs.

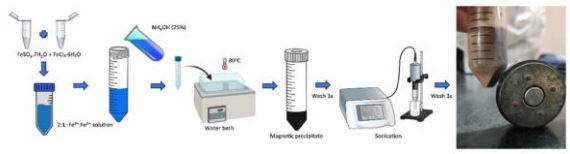

Fig. 1. Schematic diagram of magnetic nanoparticle preparation and prepared nanoparticle under the influence of magnetic field

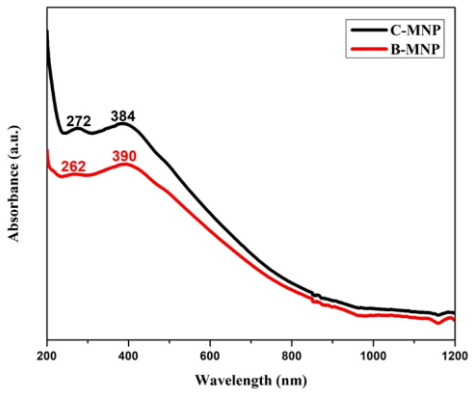

Fig. 2. Ultraviolet-visible spectra (200–1200 nm) of C-MNP and B-MNP. B-MNP, base magnetic nanoparticle; C-MNP, silica-coated magnetic nanoparticle

FTIR spectroscopy

The FTIR spectra of B-MNP and C-MNP are shown in Fig. 3. The FTIR spectrum of B-MNP exhibited various characteristic peaks corresponding to its functional groups and molecular vibrations. Notably, the broad peak at 3369 cm^{-1} corresponds to O–H stretching, and the peaks between 2950 and 2831 cm^{-1} correspond to C–H stretching vibrations. Additionally, distinct peaks were observed at 1651 and 1436 cm^{-1}, which are attributable to C=O and COO^- stretching vibrations. The following peaks were attributed to the solvent methanol, in which the MNP was stored. Additionally, peaks in the range of 1114–1020 cm^{-1}, corresponding to Fe–O stretching vibrations, along with a sharp peak at 674 cm^{-1} confirmed the presence of the Fe–O bond, which is characteristic of the MNP core structure. Notably, the FTIR spectrum of C-MNP confirmed successful silica coating on the B-MNP surface. The broad peak at 3400 and the peak at 2850 cm^{-1} is indicative of O–H and C–H stretching vibrations. Additionally, the presence of a C=O stretching vibration was confirmed by the peak at 1644 cm^{-1}. The peak at 1451 cm^{-1} was attributed to the C–H bending vibrations, while Si–O–Si asymmetric stretching vibrations appeared between 1155 and 1077 cm^{-1}. The peak at 726 cm^{-1} was attributed to Si–O–Si symmetric stretching, further supporting the successful functionalization of the nanoparticle surface. These silica-specific peaks in the C-MNP spectrum confirmed the successful silica coating of B-MNP, thereby demonstrating the effective surface functionalization.

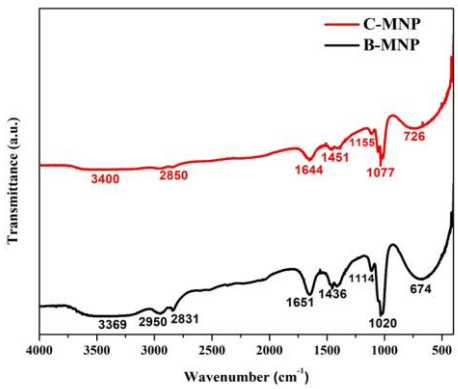

Fig. 3. Fourier-transform infrared spectra (4000–400 cm–1) of C-MNP and B-MNP. B-MNP, base magnetic nanoparticle; C-MNP, silica-coated magnetic nanoparticle

FESEM-EDAX

Notably, the results of FESEM-EDAX analyses of B-MNP and C-MNP are presented in Fig. 4A and 4B,

respectively. The FESEM images (Fig. 4A, above panel) showed that the morphology of B-MNP exhibited a relatively uniform distribution of spherical nanoparticles, along with slight agglomeration. Most of the particles presented nearly uniform morphology, with exception of agglomerates. Furthermore, the corresponding EDAX results confirmed the presence of iron as the predominant element, along with oxygen. In contrast, the FESEM images of C-MNP (Fig. 4B, above panel) showed a non-uniform morphology, along with an uneven surface. The EDAX results further revealed the presence of silicon, along with iron and oxygen, indicating that the silica coating was successfully applied on B-MNPs. The relative decrease in iron signal in C-MNP may be attributed to the extensive surface coverage by the silica coating. Altogether, these FESEM-EDS results validate the successful synthesis and structural-functional differentiation of the fabricated MNPs.

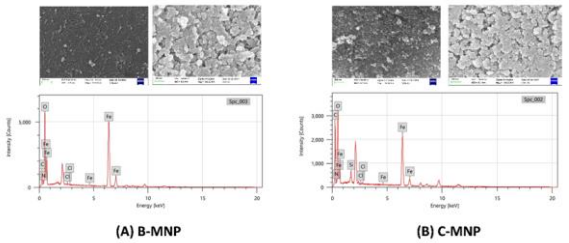

Fig. 4. Field emission scanning electron microscopy images (above) and energy-dispersive X-ray analysis results (below) for (A) B-MNP and (B) C-MNP. B-MNP, base magnetic nanoparticle; C-MNP, silica-coated magnetic nanoparticle

Zeta potential

The results of zeta potential analyses of both B-MNP and C-MNP were similar (Fig. 5A and 5B, respectively). Notably, B-MNP and C-MNP presented the zeta potential values of -24 and -31 mV, respectively. The negative values of the potential are consistent with the characteristic of both iron oxide and silica coating, with the further decrease in the value of C-MNP attributable to the successful coating of silica. Additionally, this magnitude of the negative charge suggested a higher colloidal stability and dispersion of the fabricated MNPs.

Overall, the results highlighted that both MNPs exhibited good stability, with CMP exhibiting superior results.

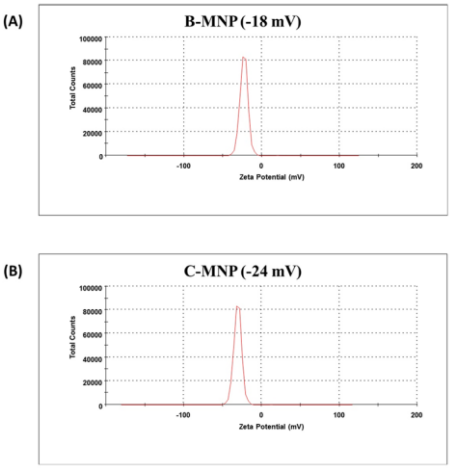

Fig. 5. Zeta potential analyses results of (A) B-MNP (−18 mV) and (B) C-MNP (−24 mV). B-MNP, base magnetic nanoparticle; C-MNP, silica-coated magnetic nanoparticle

Particle size

Particle size analysis of B-MNP and C-MNP revealed their hydrodynamic diameters (Fig. 6A and 6B, respectively). Notably, the sizes of B-MNP and C-MNP were found to be 78 and 112 nm, respectively. Additionally, size distribution graph indicated that the size of most of the particles were consistent and did not vary across a range.

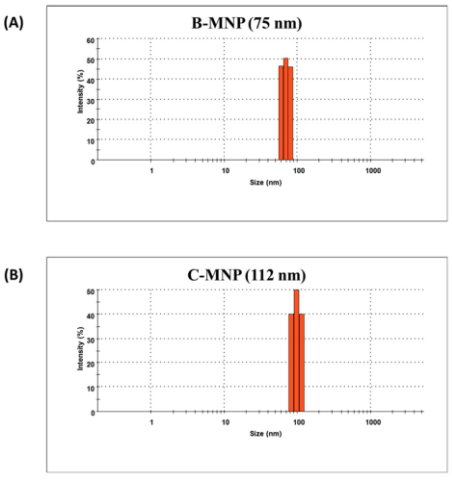

Fig. 6. Particle size analyses results of (A) B-MNP (75 nm) and (B) C-MNP (112 nm). B-MNP, base magnetic nanoparticle; C-MNP, silica-coated magnetic nanoparticle

CLSM

The results of CLSM show the successful coating of antibodies on the C-MNP surface (Fig. 7). The green fluorescence signal indicated FITC, corresponding to EpCAM primary antibody bound to the C-MNPs. The following results indicated the successful fabrication of the EpCAM antibody-bound nanosensor.

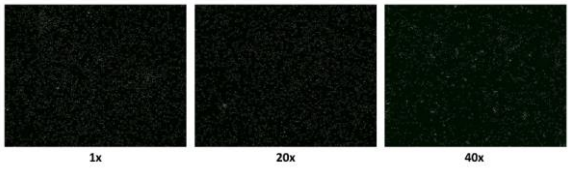

Fig. 7. Confocal laser scanning microscopy images showing successful antibody conjugation of the epithelial cell adhesion molecule antibody-functionalized silica-coated magnetic nanoparticles. Magnification: 1×, 20×, and 40×

Antibody-based immunofluorescence assay

The results of *in vitro* immunofluorescence assay (Fig. 8) showed that the EpCAM antibody effectively bound to MCF-7 cells, emitting green fluorescence owing to FITC-tagged secondary antibody. Additionally, DAPI efficiently counterstained cell nuclei, emitting blue fluorescence.

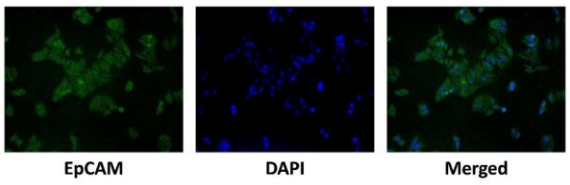

Fig. 8. Immunofluorescence assay results showing the binding of MCF-7 cells to EpCAM antibodies. Green, fluorescein isothiocyanate–EpCAM antibody; Blue, DAPI. EpCAM, epithelial cell adhesion molecule; DAPI, 4′,6-diamidino-2-phenylindole

Nanosensor-based immunofluorescence assay

The results of *in vitro* nanosensor-based immunofluorescence assay in MCF-7 and HT-29 cells are presented in Fig. 9 and 10, respectively. Notably. the cells emitted green fluorescence, indicating nanosensor binding to MCF-7 (Fig. 9A) and HT-29 cells (Fig. 10A).

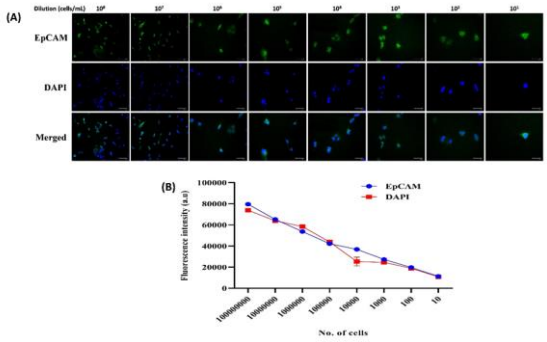

Fig. 9. EpCAM antibody-bound nanosensor-based immunofluorescence assay images (A) for MCF-7 cells (10^8–10^1 cells/mL). (B) Fluorescence readings for fluorescein isothiocyanate (FITC)–EpCAM antibody and DAPI for cell dilutions with different concentrations. Green, FITC–EpCAM antibody; Blue, DAPI. EpCAM , epithelial cell adhesion molecule; DAPI, 4′,6-diamidino-2-phenylindole

The blue fluorescence indicated nuclear staining by DAPI. Additionally, the graphs show that the fluorescence readings for EpCAM and DAPI were consistent with the dilutions of MCF-7 (Fig. 9B) and HT-29 (Fig. 10B) cell cultures (10^8–10^1 cells/mL). The fluorescence readings reduced with decreasing number of cells and indicated similar intensity between EpCAM and DAPI, which is consistent with the results observed in the images.

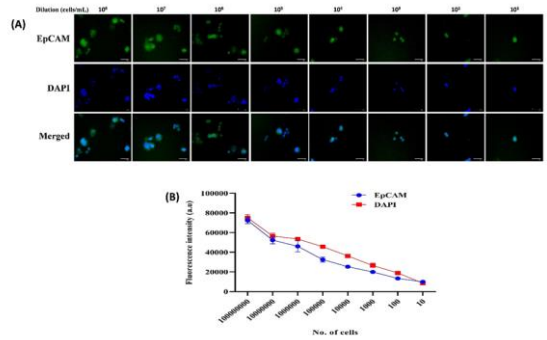

Fig. 10. EpCAM antibody-bound nanosensor-based immunofluorescence assay images (A) for HT-29 cells (10^8–10^1 cells/mL). (B) Fluorescence readings for fluorescein isothiocyanate (FITC)–EpCAM antibody and DAPI for cell dilutions with different concentrations. Green, FITC–EpCAM antibody; Blue, DAPI. EpCAM , epithelial cell adhesion molecule; DAPI, 4′,6-diamidino-2-phenylindole

DISCUSSION

This study aimed to develop magnetic nanosensors to effectively capture CTCs across multiple cancer types. The findings of this study collectively demonstrate the successful fabrication and characterization of high-performance MNPs for CTC detection and capture.

Additionally, immunofluorescence microscopy results confirmed effective CTC labeling through co-localization of the EMT marker (EpCAM; green fluorescence) and DAPI-stained nuclei (blue fluorescence), underscoring the ability of the nanosensor to detect CTCs with notable specificity. The findings underscore the potential of proposed nanosensor for further development and establishment of a CTC detection protocol.

Various studies have focused on enhancing the specificity and capture efficiency of CTCs utilizing epithelial markers, along with reporting different therapeutic targets offering enhanced CTC detetction (Peters *et al.*, 2016; Ramaker *et al.*, 2016; Rogalla and Contag, 2015). Overall, they contribute to the development and establishment of minimally invasive protocols for monitoring disease progression and therapeutic response in patients with tumors. Notably, breast cancer cells have been utilized for the characterization and evaluation of different approaches targeting the EMT-associated epithelial markers, including EpCAM (Königsberg *et al.*, 2011; Onstenk *et al.*, 2015; Weissenstein *et al.*, 2012). For instance, Suresh *et al.* investigated antibody-conjugated iron oxide nanocubes which targeted human epidermal growth factor receptor 2 and epidermal growth factor receptor. They reported that the nanocubes allowed for the capture of both epithelial and mesenchymal CTCs, further enhancing the comprehensiveness of the detection approach (Suresh *et al.*, 2020). Similarly, colon cancer cells have also been utilized in to evaluate different CTC detection approaches (Cohen *et al.*, 2006; Nicolazzo *et al.*, 2017). Altogether, these studies suggest that advances in MNP-based CTC technologies is an essential component of liquid biopsy platforms, with the potential to enhance early detection, disease prognosis, and monitoring of therapeutic efficacy across multiple cancer types.

In the present study, UV-Vis spectrum of B-MNP revealed a peak maxima at 390 nm, which is similar to the that reported previously (Parvin *et al.*, 2018). Furthermore, the peak exhibited a slight shift to 384 nm, attributable to silica coating, which has been shown to induce weak blue shifts, indicating successful nanoparticle formation and silica-coating-induced surface modification. FTIR spectra supported this by showing characteristic Si–O–Si bands and notable spectral differences suggestive of functional silica coatings; notably, the results of FTIR spectra for silica bonds were consistent with those previously reported (Santra *et al.*, 2001). FESEM images displayed spherical morphology for both B-MNP and C-MNP, with surface of B-MNP more even morphology than that of C-MNP. Additionally, EDAX confirmed the presence of silica in C-MNPs, along with a relative decrease in peak of iron, further verifying that the surface of B-MNP was successfully coated. Zeta potential analysis revealed considerable negative surface charges for both MNPs (−24 mV for B-MNP and −31 mV for C-MNP), indicating their good colloidal stability. Finally, particle size analysis revealed that the hydrodynamic diameters of B-MNP and C-MNP were 78 and 112 nm; the graph showed narrow size distributions, indicating that most of the particles were of uniform sizes. Additionally, confocal laser scanning microscopy revealed that antibody conjugation on C-MNP surfaces was successful following the coating of C-MNPs with EpCAM primary antibody, as indicated by the green fluorescent signals. Altogether, these findings validated the structural integrity, surface functionality, and stable dispersion of the developed EpCAM-antibody-bound magnetic nanosensor.

Following the successful fabrication of the nanosensors, *in vitro* immunofluorescence assays were performed in this study using MCF-7 (breast cancer) and HT-29 (colon cancer) cell lines using the antibody alone and the nanosensor. The EpCAM primary antibody effectively bound to both cells, with

green fluorescence from FITC-labeled secondary antibody denoting EpCAM, and blue fluorescence denoting DAPI-stained nuclei. Similar findings were observed for the immunofluorescence assays assessing the fabricated nanosensor in MCF-7 and HT-29 cells. The nanosensor constituted the EpCAM primary antibody, which, in turn, was bound to the FITC-tagged secondary antibody. Consistent with the results of the antibody-based immunofluorescence assay, green and blue fluorescence were recorded for EpCAM and DAPI. Additionally, the fluorescence intensities were quantitatively analyzed, revealing consistent EpCAM and DAPI signals across all serial cell dilutions (10^8–10^1 cells/mL); the signal intensity decreased proportionally with decreasing number of cancer cells. The gradual downward trend observed for fluorescence was consistent with the result found in the fluorescence microscopy images. Altogether, these assays indicated the effective specificity and sensitivity of the fabricated nanosensors.

This study has some limitations. First, the detection efficacy of the nanosensors was determined using cancer cells alone, which is different from the natural microenvironment of CTCs. Hence, the effects of interference from various other cell types and molecules on the efficacy of nanosensors need to be assessed, along with statistical significance. Notably, future investigation needs to focus on incorporating cell-spiking analyses with multiple components such as peripheral blood mononuclear cells and whole blood. Additionally, the action of fabricated nanosensors was not assessed in living organism. This prompts the need for *in vivo* study to analyze the efficacy of the nanosensors in an animal model.

CONCLUSION

Overall, MNPs have shown great potential regarding the future direction in cancer diagnostics, particularly in the detection of CTCs and monitoring metastasis for better prognosis of patients with tumors. They exhibit unique physicochemical properties, including their magnetism, a high surface area-to-volume ratio, and ease of surface modification, allowing them for highly sensitive and specific diagnostic applications. Regarding CTC detection, functionalization of MNPs with antibodies against EMT-specific markers, such as EpCAM, can offer considerable advantages in isolating rare CTCs from the blood samples through magnetic separation techniques. Moreover, this approach offers advantages of a minimally invasive, real-time method to assess tumor progression, evaluate treatment efficacy, and predict disease prognosis.

Altogether, the findings of this study demonstrate the successful fabrication of an iron oxide-based nanosensor. The fabricated MNP was successfully coated with silica to generate C-MNP, which was further functionalized with EpCAM antibody. The proposed nanosensor presented notable stability and could effectively detected different cancer cell lines. The proposed method provides a strong research basis for further protocol development for effective detection of CTCs to improve cancer diagnostics and monitoring of metastasis development. Future studies on the application of MNPs for diagnostic and therapeutic purposes need to integrate fluorescence-based approaches with other technologies, such as magnetic resonance imaging, flow cytometry, and photoacoustic imaging, along with other surface markers to enhance the visualization and quantification of metastatic sites.

Furthermore, advances need to be made in biosensor design, integrating approaches such as microfluidics and machine learning, to establish MNP-based assays as an automated, miniaturized, and accurate testing tool for cancer therapy and diagnostics.

ACKNOWLEDGEMENTS

This study was financially supported by the DST-INSPIRE fellowship, Department of Science and Technology, Government of India, India (Grant number DST/INSPIRE/03/2021/002275); and Chief Minister Research Grant-2023, Government of Tamil Nadu, India (Grant number CMRG2023BBB08058).

REFERENCES

Baeuerle PA, Gires O. 2007. EpCAM (CD326) finding its role in cancer. British Journal of Cancer **96**, 417–423. https://doi.org/10.1038/sj.bjc.6603494

Chang Z, Wang Z, Shao D, Yue J, Xing H, Li L, Ge M, Li M, Yan H, Hu H, Xu Q, Dong W. 2018. Shape engineering boosts magnetic mesoporous silica nanoparticle-based isolation and detection of circulating tumor cells. ACS Applied Materials & Interfaces **10**, 10656–10663. https://doi.org/10.1021/acsami.7b19325

Chauhan A, Kaur R, Ghoshal S, Pal A. 2021. Exploration of circulating tumour cell (CTC) biology: A paradigm shift in liquid biopsy. Indian Journal of Clinical Biochemistry **36**, 131–142. https://doi.org/10.1007/s12291-020-00923-4

Cho H, Indig GL, Weichert J, Shin HC, Kwon GS. 2012. *In vivo* cancer imaging by poly(ethylene glycol)-b-poly(ε-caprolactone) micelles containing a near-infrared probe. Nanomedicine: Nanotechnology, Biology and Medicine **8**, 228–236. https://doi.org/10.1016/j.nano.2011.06.009

Cimino A, Halushka M, Illei P, Wu X, Sukumar S, Argani P. 2010. Epithelial cell adhesion molecule (EpCAM) is overexpressed in breast cancer metastases. Breast Cancer Research and Treatment **123**, 701–708. https://doi.org/10.1007/s10549-009-0671-z

Cohen SJ, Alpaugh RK, Gross S, O'Hara SM, Smirnov DA, Terstappen LWMM, Allard WJ, Bilbee M, Cheng JD, Hoffman JP, Lewis NL, Pellegrino A, Rogatko A, Sigurdson E, Wang H, Watson JC, Weiner LM, Meropol NJ. 2006. Isolation and characterization of circulating tumor cells in patients with metastatic colorectal cancer. Clinical Colorectal Cancer **6**, 125–132. https://doi.org/10.3816/CCC.2006.n.029

Debnath P, Huirem RS, Dutta P, Palchaudhuri S. 2022. Epithelial–mesenchymal transition and its transcription factors. Bioscience Reports **42**, BSR20211754. https://doi.org/10.1042/BSR20211754

Ding N, Sano K, Kanazaki K, Ohashi M, Deguchi J, Kanada Y, Ono M, Saji H. 2016. In vivo HER2-targeted magnetic resonance tumor imaging using iron oxide nanoparticles conjugated with anti-HER2 fragment antibody. Molecular Imaging and Biology **18**, 870–876. https://doi.org/10.1007/s11307-016-0977-2

Ferlay J, Ervik M, Lam F, Laversanne M, Colombet M, Piñeros M, Znaor A, Soerjomataram I, Bray F. 2024. Global cancer observatory: Cancer today. International Agency for Research on Cancer. https://gco.iarc.who.int/media/globocan/factsheets/cancers/39-all-cancers-fact-sheet.pdf

Garg M. 2013. Epithelial-mesenchymal transition – activating transcription factors – multifunctional regulators in cancer. World Journal of Stem Cells **5**, 188–195. https://doi.org/10.4252/wjsc.v5.i4.188

Gerstberger S, Jiang Q, Ganesh K. 2023. Metastasis. Cell **186**, 1564–1579. https://doi.org/10.1016/j.cell.2023.03.003

Gonzalez DM, Medici D. 2014. Signaling mechanisms of the epithelial-mesenchymal transition. Science Signaling **7**, re8. https://doi.org/10.1126/scisignal.2005189

Huang X, O'Connor R, Kwizera EA. 2017. Gold nanoparticle based platforms for circulating cancer marker detection. Nanotheranostics **1**, 80–102. https://doi.org/10.7150/ntno.18216

Imrich S, Hachmeister M, Gires O. 2012. EpCAM and its potential role in tumor-initiating cells. Cell Adhesion & Migration **6**, 30–38. https://doi.org/10.4161/cam.18953

Jia F, Wang Y, Fang Z, Dong J, Shi F, Zhang W, Wang Z, Hu Z. 2021. Novel peptide-based magnetic nanoparticle for mesenchymal circulating tumor cells detection. Analytical Chemistry **93**, 5670–5675.
https://doi.org/10.1021/acs.analchem.1c00577

Königsberg R, Obermayr E, Bises G, Pfeiler G, Gneist M, Wrba F, de Santis M, Zeillinger R, Hudec M, Dittrich C. 2011. Detection of EpCAM positive and negative circulating tumor cells in metastatic breast cancer patients. Acta Oncologica **50**, 700–710.
https://doi.org/10.3109/0284186X.2010.549151

Kwak B, Lee J, Lee D, Lee K, Kwon O, Kang S, Kim Y. 2017. Selective isolation of magnetic nanoparticle-mediated heterogeneity subpopulation of circulating tumor cells using magnetic gradient based microfluidic system. Biosensors and Bioelectronics **88**, 153–158.
https://doi.org/10.1016/j.bios.2016.08.002

Lamouille S, Xu J, Derynck R. 2014. Molecular mechanisms of epithelial–mesenchymal transition. Nature Reviews Molecular Cell Biology **15**, 178–196.
https://doi.org/10.1038/nrm3758

Lianidou E, Pantel K. 2019. Liquid biopsies. Genes, Chromosomes and Cancer **58**, 219–232.
https://doi.org/10.1002/gcc.22695

Liu Y, Li R, Zhang L, Guo S. 2022. Nanomaterial-based immunocapture platforms for the recognition, isolation, and detection of circulating tumor cells. Frontiers in Bioengineering and Biotechnology **10**, 850241. https://doi.org/10.3389/fbioe.2022.850241

Marciello M, Luengo Y, Morales MP. 2016. Iron oxide nanoparticles for cancer diagnosis and therapy. In: Nanoarchitectonics for smart delivery and drug targeting (pp. 667–694). Elsevier.
https://doi.org/10.1016/B978-0-323-47347-7.00024-0

Medley CD, Bamrungsap S, Tan W, Smith JE. 2011. Aptamer-conjugated nanoparticles for cancer cell detection. Analytical Chemistry **83**, 727–734.
https://doi.org/10.1021/ac102263v

Myung JH, Tam KA, Park S, Cha A, Hong S. 2016. Recent advances in nanotechnology-based detection and separation of circulating tumor cells. WIREs Nanomedicine and Nanobiotechnology **8**, 223–239.
https://doi.org/10.1002/wnan.1360

Nicolazzo C, Raimondi C, Francescangeli F, Ceccarelli S, Trenta P, Magri V, Marchese C, Zeuner A, Gradilone A, Gazzaniga P. 2017. EpCAM-expressing circulating tumor cells in colorectal cancer. The International Journal of Biological Markers **32**, 415–420.
https://doi.org/10.5301/ijbm.5000284

Onstenk W, Kraan J, Mostert B, Timmermans MM, Charehbili A, Smit VTHBM, Kroep JR, Nortier JWR, van de Ven S, Heijns JB, Kessels LW, van Laarhoven HWM, Bos MMEM, van de Velde CJH, Gratama JW, Sieuwerts AM, Martens JWM, Foekens JA, Sleijfer S. 2015. Improved circulating tumor cell detection by a combined EpCAM and MCAM CellSearch enrichment approach in patients with breast cancer undergoing neoadjuvant chemotherapy. Molecular Cancer Therapeutics **14**, 821–827.
https://doi.org/10.1158/1535-7163.MCT-14-0653

Opoku-Damoah Y, Assanhou AG, Sooro MA, Baduweh CA, Sun C, Ding Y. 2018. Functional diagnostic and therapeutic nanoconstructs for efficient probing of circulating tumor cells. ACS Applied Materials & Interfaces **10**, 14231–14247.
https://doi.org/10.1021/acsami.7b17896

Pantel K, Speicher MR. 2016. The biology of circulating tumor cells. Oncogene **35**, 1216–1224.
https://doi.org/10.1038/onc.2015.192

Parvin F, Nayna OK, Tareq SM, Rikta SY, Kamal AK. 2018. Facile synthesis of iron oxide nanoparticle and synergistic effect of iron nanoparticle in the presence of sunlight for the degradation of DOM from textile wastewater. Applied Water Science **8**, 73. https://doi.org/10.1007/s13201-018-0719-5

Peters ITA, Hilders CGJM, Sier CFM, Vahrmeijer AL, Smit VTHBM, Baptist Trimbos J, Kuppen PJK. 2016. Identification of cell-surface markers for detecting breast cancer cells in ovarian tissue. Archives of Gynecology and Obstetrics **294**, 385–393. https://doi.org/10.1007/s00404-016-4036-7

Ramaker K, Bade S, Röckendorf N, Meckelein B, Vollmer E, Schultz H, Fröschle GW, Frey A. 2016. Absence of the epithelial glycocalyx as potential tumor marker for the early detection of colorectal cancer. PLOS ONE **11**, e0168801. https://doi.org/10.1371/journal.pone.0168801

Riethdorf S, O'Flaherty L, Hille C, Pantel K. 2018. Clinical applications of the CellSearch platform in cancer patients. Advanced Drug Delivery Reviews **125**, 102–121. https://doi.org/10.1016/j.addr.2018.01.011

Rogalla S, Contag CH. 2015. Early cancer detection at the epithelial surface. The Cancer Journal **21**, 179–187. https://doi.org/10.1097/PPO.0000000000000122

Santra S, Tapec R, Theodoropoulou N, Dobson J, Hebard A, Tan W. 2001. Synthesis and characterization of silica-coated iron oxide nanoparticles in microemulsion: the effect of nonionic surfactants. Langmuir **17**, 2900–2906. https://doi.org/10.1021/la0008636

Spizzo G, Fong D, Wurm M, Ensinger C, Obrist P, Hofer C, Mazzoleni G, Gastl G, Went P. 2011. EpCAM expression in primary tumour tissues and metastases: an immunohistochemical analysis. Journal of Clinical Pathology **64**, 415–420. https://doi.org/10.1136/jcp.2011.090274

Steinestel K, Eder S, Schrader AJ, Steinestel J. 2014. Clinical significance of epithelial–mesenchymal transition. Clinical and Translational Medicine **3**, e17. https://doi.org/10.1186/2001-1326-3-17

Suresh D, Ghoshdastidar S, Gangula A, Mukherjee S, Upendran A, Kannan R. 2020. Magnetic iron nanocubes effectively capture epithelial and mesenchymal cancer cells. ACS Omega **5**, 23724–23735. https://doi.org/10.1021/acsomega.0c02699

Van der Toom EE, Verdone JE, Gorin MA, Pienta KJ. 2016. Technical challenges in the isolation and analysis of circulating tumor cells. Oncotarget **7**, 62754–62766. https://doi.org/10.18632/oncotarget.11191

Weissenstein U, Schumann A, Reif M, Link S, Toffol-Schmidt UD, Heusser P. 2012. Detection of circulating tumor cells in blood of metastatic breast cancer patients using a combination of cytokeratin and EpCAM antibodies. BMC Cancer **12**, 206. https://doi.org/10.1186/1471-2407-12-206

Wenqi D, Li W, Shanshan C, Bei C, Yafei Z, Feihu B, Jie L, Daiming F. 2009. EpCAM is overexpressed in gastric cancer and its downregulation suppresses proliferation of gastric cancer. Journal of Cancer Research and Clinical Oncology **135**, 1277–12853.https://doi.org/10.1007/s00432-009-0569-5

Williams SCP. 2013. Circulating tumor cells. Proceedings of the National Academy of Sciences **110**, 4861–4861. https://doi.org/10.1073/pnas.1304186110

Yang J, Antin P, Berx G, Blanpain C, Brabletz T, Bronner M, Campbell K, Cano A, Casanova J, Christofori G, Dedhar S, Derynck R, Ford HL, Fuxe J, García de Herreros A, Goodall GJ, Hadjantonakis AK, Huang RYJ, Kalcheim C, Kalluri R, Kang Y, Khew-Goodall Y, Levine H, Liu J, Longmore GD, Mani SA, Massagué J, Mayor R, McClay D, Mostov KE, Newgreen DF, Nieto MA, Puisieux A, Runyan R, Savagner P, Stanger B, Stemmler MP, Takahashi Y, Takeichi M, Theveneau E, Thiery JP, Thompson EW, Weinberg RA, Williams ED, Xing J, Zhou BP, Sheng G; EMT International Association (TEMTIA). 2020. Guidelines and definitions for

research on epithelial–mesenchymal transition. Nature Reviews Molecular Cell Biology **21**, 341–352. https://doi.org/10.1038/s41580-020-0237-9

Yang Y, Huang G, Lian J, Long C, Zhao B, Liu X, Zhang B, Ye W, Chen J, Du L, Jiang Z, Liu J, Zhang J, Hu C, Chen Q, Hong X. 2024. Circulating tumour cell clusters: isolation, biological significance and therapeutic implications. BMJ Oncology **3**, e000437. https://doi.org/10.1136/bmjonc-2024-000437

Yao D, Dai C, Peng S. 2011. Mechanism of the mesenchymal–epithelial transition and its relationship with metastatic tumor formation. Molecular Cancer Research **9**, 1608–1620. https://doi.org/10.1158/1541-7786.MCR-10-0568

Zhou L, Zhu Y. 2018. The EpCAM overexpression is associated with clinicopathological significance and prognosis in hepatocellular carcinoma patients: A systematic review and meta-analysis. International Journal of Surgery **56**, 274–280. https://doi.org/10.1016/j.ijsu.2018.06.025

Zhou S, Xu H, Duan Y, Tang Q, Huang H, Bi F. 2024. Survival mechanisms of circulating tumor cells and their implications for cancer treatment. Cancer and Metastasis Reviews **43**, 941–957. https://doi.org/10.1007/s10555-024-10178-7

Zhu Y, Kekalo K, NDong C, Huang Y, Shubitidze F, Griswold KE, Baker I, Zhang JXJ. 2016. Magnetic-nanoparticle-based immunoassays-on-chip: materials synthesis, surface functionalization, and cancer cell screening. Advanced Functional Materials **26**, 3953–3972. https://doi.org/10.1002/adfm.201504176